

# Photoinduced Segregation Behavior in 2D Mixed Halide Perovskite: Effects of Light and Heat

Tik Lun Leung,<sup>‡</sup> Zhilin Ren,<sup>‡</sup> Ali Asgher Syed, Luca Grisanti, Aleksandra B. Djurišić,\* Jasminka Popović\*

Photoinduced halide segregation (PHS) is a process of critical importance for the performance of perovskite solar cells with mixed halide absorber layers. However, PHS is still not well understood, especially in the case of layered mixed halide perovskites (MHPs), which are less commonly studied compared to their 3D counterparts. Here, we investigated temperature- and light-induced PHS in 2D MHPs with a phenylpropylammonium (PPA) spacer. We found that 2D PPA- based MHPs exhibited complex segregation behavior dependence on temperature and illumination intensity with the suppression of segregation observed at high temperature (attributed to the highly exothermic nature of the process) as well as moderate illumination intensities, illustrating the importance of additional processes present in this particular material, which exhibits distinctly different behavior compared to 2D MHPs with other aromatic cations.

Metal halide perovskites have widely tunable bandgaps by simple composition adjustments. They have a general formula of  $ABX_3$ , where A = MA, FA, or Cs, B = Sn or Pb, and X = I, Br, or Cl. With different combinations of A, B, and X ions, the bandgap can be varied from 1.24 to 3.55 eV.<sup>1</sup> The wide range of bandgap tunability, coupled with versatile preparation procedures, enables new solutions to existing challenges such as deep blue light emitting diodes (LEDs)<sup>2,3</sup> and multijunction photovoltaics (PVs).<sup>4-6</sup> While the multijunction perovskite-Si tandem cells have recently reached a power conversion efficiency (PCE) of 29.5%,<sup>7</sup> exceeding the theoretical limit of the single silicon cell,<sup>8</sup> challenges remain in terms of device stability. The ideal bandgap of the top absorber in a tandem cell is about 1.7 eV, which can be easily achieved by the halide mixing method. However, mixed halide perovskites (MHPs), noted as  $AB(I_{1-x}Br_x)_3$ , are commonly observed to segregate under illumination; i.e., they exhibit photoinduced halide segregation (PHS) to form iodide-rich and bromide-rich domains.<sup>9</sup> The segregation can lead to rapid degradation in devices,<sup>10</sup> and the iodide-rich domain with lower bandgap energy behaves as a carrier sink, which can cause an open-circuit voltage ( $V_{oc}$ ) deficit.<sup>11</sup> Although the correlation

between vacancy and PHS has been evidenced,<sup>12,13</sup> the mechanisms of PHS are still not well understood.

Different models have been proposed to describe PHS. The two commonly used models are the thermodynamic miscibility gap model<sup>14,15</sup> and the polaron model.<sup>16,17</sup> According to the miscibility gap model,<sup>14,15</sup> PHS is a thermodynamic governed process where the illumination can provide energy to overcome the energy barrier of separating the mixed phase, and halide segregation does not occur when the illumination drops below the threshold intensity, which is determined by material properties and the temperature. In a polaron model,<sup>16,17</sup> segregation is a carrier-driven process where the energy difference of the parent mixed phase and lower bandgap phases lead to carrier funneling, which coupled with the lattice structure, induces polaron formation. Neither of the two common models is fully able to explain the contradictory

experimental observations simultaneously, namely, remixing of the segregated phases at high temperature<sup>18,19</sup> and the insensitivity of the terminal composition to temperature.<sup>20</sup> Another thermodynamic model, the thermodynamic energy bandgap model,<sup>20</sup> which attempted to reconcile the predictions of the two models, predicted a terminal composition close to zero, and the difference with the experimental observations was attributed to kinetic limitations and a temperature-independent percolation threshold.<sup>20</sup> In addition to differences in the prediction of the terminal composition and its temperature dependence, the predicted illumination values for illumination suppression also vary greatly with low illumination levels ( $\sim 20$  to  $230 \mu\text{W cm}^{-2}$ ) estimated by the miscibility gap and high illumination levels ( $0.75$  to  $200 \text{ W cm}^{-2}$ ) estimated by the polaron model. In addition, the importance of hole trapping and the oxidation of iodide species has been recently recognized.<sup>21,22</sup> Obviously, further refinement of PHS models is necessary due to their complex nature, which includes several factors that cannot be easily distinguished.

In addition, while PHS in 3D perovskites is widely investigated, limited knowledge exists for PHS and ion migration in layered Ruddlesden–Popper (RP) and/or Dion–Jacobson (DJ) perovskites,<sup>23–30</sup> which have a general formula of  $\text{L}_2\text{A}_{n-1}\text{B}_n\text{X}_{3n+1}$  (RP) or  $\text{LA}_{n-1}\text{B}_n\text{X}_{3n+1}$  (DJ), where L is the bulky organic spacer cation and  $n$  is the number of octahedral lead halide layers sandwiched between spacer cation bilayers. Similar to 3D perovskites, the divergence between different PHS models persists in these materials as well, and its interpretation is further aggravated by the effect that the choice of the spacer cation has on the PHS, which is absent in 3D perovskites. Despite increased complexity, the elucidation of processes occurring in 2D MPH is particularly important since those materials demonstrated significant ability to suppress the halide segregation. Several spacer cations were found to impede halide segregation, for example, the butylammonium (BA) spacer for electric field driven halide segregation in LEDs<sup>23</sup> and the benzylammonium (BZA) spacer for PHS under  $200 \text{ mW cm}^{-2}$  LED light soaking at  $85 \text{ }^\circ\text{C}$ .<sup>24</sup> Furthermore, a rigid spacer of phenethylammonium (PEA) was found to significantly suppress PHS in a 2D MHP, compared with the BA spacer.<sup>25</sup> Thus, it is critical to improve our understanding of the PHS to fully utilize the use of a 2D MHP to develop PHS-resistant devices. Unfortunately, the problems with different models developed for PHS in 3D perovskites also extend to their 2D counterparts. For example, the activation energy of PHS in  $\text{PEA}_2\text{Pb}(\text{Br}_{0.5}\text{I}_{0.5})_4$  was  $21.7 \text{ kJ mol}^{-1}$ , which is smaller than that in  $\text{MAPb}(\text{Br}_{0.5}\text{I}_{0.5})_3$  ( $28.9 \text{ kJ mol}^{-1}$ ),<sup>18,26</sup> which would indicate that PHS in  $\text{PEA}_2\text{Pb}(\text{Br}_{0.5}\text{I}_{0.5})_4$  would be more pronounced compared to that in  $\text{MAPb}(\text{Br}_{0.5}\text{I}_{0.5})_3$ , different from experimental observations. Recently, a study on the mixing–demixing process in  $(\text{PDMA})\text{Pb}(\text{Br}_{0.5}\text{I}_{0.5})_4$  (PDMA: 1,4-phenylenedimethan ammonium) thin film revealed a miscibility gap under illumination, which supports the idea that the process is governed by thermodynamics rather than kinetics.<sup>27</sup> This implies that the segregation resistance cannot be evaluated by comparing the activation energies in different MHPs due to different experimental conditions, such as sample preparation methods (which would affect the grain sizes and defect levels in the samples and consequently ion migration) and illumination intensities. It has been well recognized that there are still several unanswered questions concerning PHS and that the analysis is complicated by conflicting data in the literature.<sup>31,32</sup>

To rationalize the diverging phenomena, we investigate the PHS dependence on temperature and illumination intensity in a 2D MHP. We have developed an *in situ* absorption measurement to monitor the halide composition of a 2D MHP with a phenylpropylammonium (PPA) spacer under illumination. Since it has been shown that layered perovskites with aromatic and aliphatic spacer cations show distinctly different behaviors<sup>25</sup> and that PHS and ion migration are strongly dependent on the spacer cation used,<sup>25,29,30</sup> we have chosen the PPA cation as an aromatic spacer with a longer alkyl chain tail compared to more commonly studied PEA. As shown in Figures S1 and S2, the PPA-based perovskite exhibits significantly different behavior compared to both BZA and PEA; for PEA, we observe suppressed segregation at both  $25$  and  $84 \text{ }^\circ\text{C}$  and, for BZA, we observe no suppression at both temperatures, while for PPA, we observe suppression only at  $84 \text{ }^\circ\text{C}$  (for a given illumination intensity of  $6.5 \text{ mW/cm}^2$ ). This makes PPA an excellent candidate for performing a comprehensive investigation of PHS as a function of both temperature and light intensity, as it has potential to uncover a complex behavior that can eventually lead to a better understanding of this important phenomenon. In addition, the investigation of PHS over a wide range of temperature and illumination intensities is important as the solar cells operating outdoors will be exposed to a wide range of conditions and those operating indoors (perovskite solar cells are particularly promising for indoor applications<sup>33,34</sup>) are operating at significantly lower illumination intensities compared to 1 sun ( $100 \text{ mW/cm}^2$ ).

A complex dependence of the segregation on temperature and illumination intensity was indeed observed for this material for the investigated illumination power ( $6.5$ – $100 \text{ mW/cm}^2$ ) and temperature ( $25$ – $84 \text{ }^\circ\text{C}$ ). The segregation process was then interpreted in the aspects of kinetics and thermodynamics with Arrhenius and Van’t Hoff equations, respectively. At the lowest illumination intensity ( $6.5 \text{ mW/cm}^2$ ), the photoinduced segregation can be well described by the Van’t Hoff equation. With the increase of illumination intensity, other mechanisms start to dominate the process and a more complex behavior emerges, which can no longer be approximated by a simple linear function. At rarely considered moderate illumination intensities of around 0.1 sun, a particularly interesting behavior of segregation suppression at both high temperature and increased illumination intensity was found, which was attributed to the thermodynamic nature of PHS, instead of its kinetic property. A further increase of the illumination intensity, however, leads to re-emergence of segregation, which can be attributed to increased effects of hole trapping and/or polaron-induced strain. Interestingly, the segregation at high intensity can be described by a biexponential process at lower temperatures, but it can be described with a single exponential function again at  $84 \text{ }^\circ\text{C}$ .

The 2D perovskite film of  $\text{PPA}_2\text{Pb}(\text{Br}_{0.5}\text{I}_{0.5})_4$  was deposited on a glass substrate by spin-coating in an argon filled glovebox. Pure bromide and pure iodide 2D perovskite thin films were also prepared as references. A homogeneously mixed halide perovskite was obtained, as evidenced by the exciton peak at  $450 \text{ nm}$  in the absorption spectrum (Figure S3), which is in agreement with other 2D mixed halide perovskites (MHPs).<sup>25,26</sup> The XRD patterns of  $\text{PPA}_2\text{PbI}_4$ ,  $\text{PPA}_2\text{PbBr}_4$ , and  $\text{PPA}_2\text{Pb}(\text{Br}_{0.5}\text{I}_{0.5})_4$  are shown in Figure S4. Although bromide is smaller than iodide, the  $\text{PPA}_2\text{PbBr}_4$  structure exhibits a larger periodicity along the  $c$ -direction ( $d = 19.35 \text{ \AA}$ )

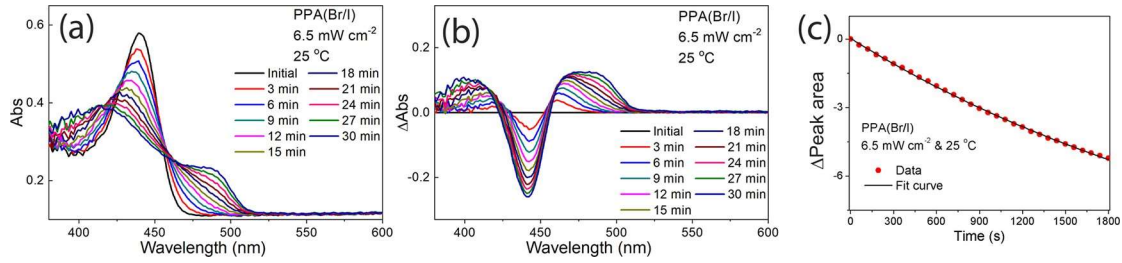


Figure 1. (a) *In situ* absorption spectra recorded at different times during the segregation process of  $\text{PPA}_2\text{Pb}(\text{Br}_{0.5}\text{I}_{0.5})_4$  at 25 °C under a xenon lamp with  $6.5 \text{ mW cm}^{-2}$ ; (b) absorption difference spectra and (c) segregation trace.

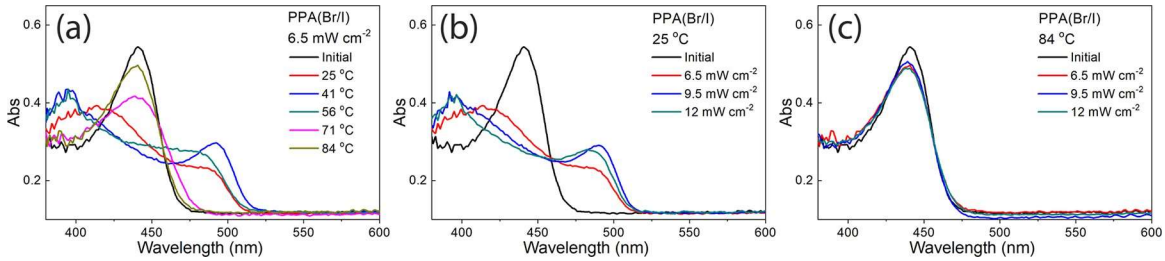
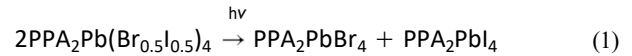


Figure 2. *In situ* absorption spectra of  $\text{PPA}_2\text{Pb}(\text{Br}_{0.5}\text{I}_{0.5})_4$  recorded at  $t = 0 \text{ s}$  and exposed to a xenon lamp for 30 min under different conditions: (a)  $T = 25, 41, 56, 71,$  and  $84 \text{ °C}$  at  $6.5 \text{ mW cm}^{-2}$  and (b)  $T = 25 \text{ °C}$  and (c)  $T = 84 \text{ °C}$  at  $6.5, 9.5,$  and  $12.0 \text{ mW cm}^{-2}$ .

compared to  $\text{PPA}_2\text{PbI}_4$ , which exhibits a periodicity of  $d = 16.9 \text{ \AA}$ . This indicates that the packing of the spacer cations and the intermolecular interactions within the bilayer have a stronger influence on the contraction/expansion of the unit cell than the difference in sizes of the halide ions. This is often not the case with an alkylammonium spacer, such as butylammonium, but various types of  $\pi$ - $\pi$  interactions that can be established when alkylphenylammonium spacers are used seem to have a prevailing effect on the overall size of the unit cell. The same as in the case of PPA, the smaller unit was reported for the iodide structure with phenylethylammonium (PEA) compared to its bromide analogue.<sup>35,36</sup> So, while the pure bromide shows a larger interlayer distance than the pure iodide PPA-based perovskite, the interlayer distance of PPA MHP ( $d = 19.51 \text{ \AA}$ ) exceeds those of both pure halide perovskites. Since the difference between  $\text{PPA}_2\text{PbI}_4$ ,  $\text{PPA}_2\text{PbBr}_4$ , and  $\text{PPA}_2\text{Pb}(\text{Br}_{0.5}\text{I}_{0.5})_4$  is not caused only by the (partial) substitution of halides on the crystallographic B site, but instead, also includes the reorganization of the spacer bilayer accompanied by the conformational changes of the PPA cations, Vegard's law is not applicable, thus making XRD an unsuitable method to investigate PHS. In order to continuously follow the PHS and prevent the remixing process in the dark, the *in situ* visible absorption measurements with a xenon lamp as the excitation source and AM0 filter were conducted (Figure S5). Films were encapsulated with cover glass and epoxy to prevent potential degradation due to oxygen and moisture.<sup>37</sup> The absorption spectra were obtained from the light transmittance by the Beer-Lambert law. The obtained *in situ* absorption exhibits a minor blue-shift in the exciton peak when compared to the steady-state absorption spectrum [Figure S6].

Figure 1a shows the *in situ* absorption spectra of the  $\text{PPA}_2\text{Pb}(\text{Br}_{0.5}\text{I}_{0.5})_4$  film at 25 °C for 30 min. Under prolonged illumination, the intensity of the exciton peak at 443.0 nm decreases and blue-shifts with a simultaneous increase of absorption intensity at longer wavelengths. Blue-shifting of the parent peak indicates bromide enrichment in the parent phase while the emerging absorption implies the formation of an

iodide-rich phase. The segregation process can be described by eq 1



This observation resembles the PHS in 2D MHPs with other spacer cations.<sup>25,26</sup> Also, the newly evolved exciton peak at longer wavelength agrees with the formation of the iodide-rich phase during halide segregation.<sup>15,38</sup> The increased peak width suggests that the segregated sample is composed of a wide range of halide compositions. To visualize the composition changes, the absorption difference spectrum was obtained by subtracting the initial spectrum (Figure 1b). The absorption difference spectrum clearly exhibits a depletion of the parent composition, accompanied by the growth of bromide-rich and iodide-rich phases. The equilibrium state between the mixed and segregated phases can be revealed by two isosbestic points at 422 nm for the mixed bromide-rich phases and 456 nm for the mixed iodide-rich phases. The composition change was quantified by integrating the peak area in the absorption difference spectrum and plotted as a segregation trace (Figure 1c). The trace was fit with a monoexponential function; the pseudo-first-order rate constant ( $k$ ) of  $3.04 \times 10^{-4} \text{ s}^{-1}$  was obtained. The obtained rate constant is comparable to the value obtained with the  $\text{PEA}_2\text{Pb}(\text{Br}_{0.5}\text{I}_{0.5})_4$  film ( $<4 \times 10^{-4} \text{ s}^{-1}$  at  $100 \text{ mW cm}^{-2}$  and 295 K),<sup>26</sup> and it is an order of magnitude smaller than that with the  $(\text{PDMA})\text{Pb}(\text{Br}_{0.5}\text{I}_{0.5})_4$  film ( $6 \times 10^{-2} \text{ s}^{-1}$  at  $1.5 \text{ mW cm}^{-2}$  and 313 K);<sup>27</sup> however, neither of them showed obvious segregation in the given conditions. Thus, it should be noted that the degree of segregation cannot be revealed by the rate of reaction.

The photoinduced halide segregation process in the  $\text{PPA}_2\text{Pb}(\text{Br}_{0.5}\text{I}_{0.5})_4$  films was further investigated at elevated temperatures. The *in situ* absorption spectra, absorption difference spectra, and corresponding segregation traces recorded at different times during the segregation process of  $\text{PPA}_2\text{Pb}(\text{Br}_{0.5}\text{I}_{0.5})_4$  at  $T = 41, 56, 71,$  and  $84 \text{ °C}$  under a xenon lamp with  $6.5 \text{ mW cm}^{-2}$  are shown in Figure S7. With an increase in temperature, the rate constant increases from 3.04

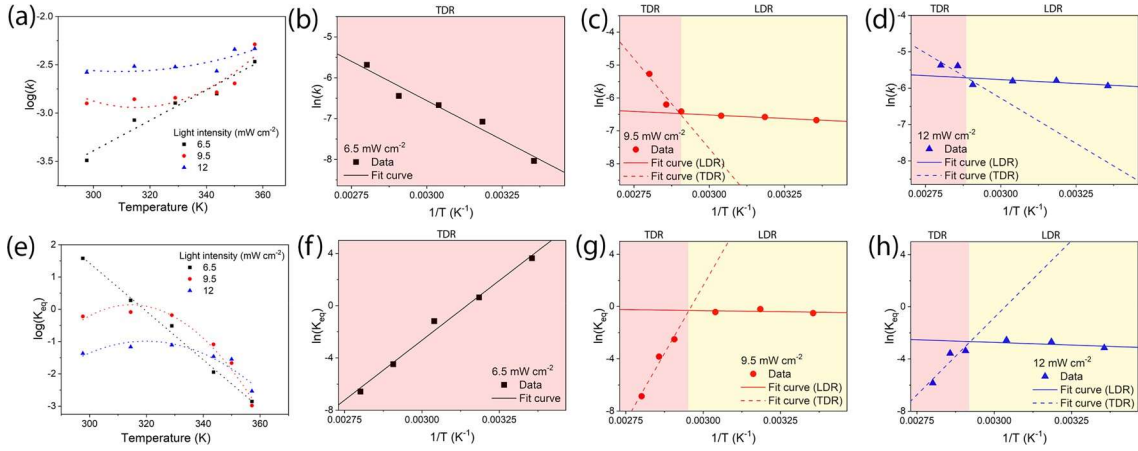


Figure 3. (a)  $\log(k)$  versus temperature plot and Arrhenius plots for the photoinduced halide segregation processes in the  $\text{PPA}_2\text{Pb}(\text{Br}_{0.5}\text{I}_{0.5})_4$  film at  $T = 25, 41, 56, 71,$  and  $84^\circ\text{C}$  under (b)  $6.5\text{ mW cm}^{-2}$ , (c)  $9.5\text{ mW cm}^{-2}$ , and (d)  $12.0\text{ mW cm}^{-2}$ . (e)  $\log(K_{\text{eq}})$  versus temperature plot and Van't Hoff plots of the  $\text{PPA}_2\text{Pb}(\text{Br}_{0.5}\text{I}_{0.5})_4$  film at  $T = 25, 41, 56, 71,$  and  $84^\circ\text{C}$  under (f)  $6.5\text{ mW cm}^{-2}$ , (g)  $9.5\text{ mW cm}^{-2}$ , and (h)  $12.0\text{ mW cm}^{-2}$ . The polynomial fit curves (dashed line) show that data are converging at a high temperature. Solid lines are linear fit of the data. Red and yellow shadings indicate the temperature dominated region (TDR) and light dominated region (LDR), respectively.

$\times 10^{-4}\text{ s}^{-1}$  at  $T = 25^\circ\text{C}$  to  $3.36 \times 10^{-3}\text{ s}^{-1}$  at  $T = 84^\circ\text{C}$ . The influence of temperature on the rate constant can be expressed with the Arrhenius equation (eq 2):<sup>18</sup>

$$\ln(k) = \frac{E_a}{RT} + \ln(A) \quad (2)$$

where  $A$  is a pre-exponential factor,  $E_a$  is the activation energy of the photoinduced halide segregation process,  $R$  is the universal gas constant, and  $T$  is the temperature, as shown in Figure 3b. Although the rate of segregation reaction increases with temperature, as can also be seen from the Arrhenius diagram where  $\ln(k)$  decreases linearly with  $1/T$ , one should always keep in mind that the reaction rate itself does not address the extent of the segregation reaction, as this is actually controlled by thermodynamic factors (*vide infra*). This is seen at the highest temperatures where the reaction rates are the largest while the segregation is almost suppressed. Figure 2a shows almost no bromide enrichment of the parent phase nor the formation of an iodide-rich phase at the temperatures of 71 and  $84^\circ\text{C}$ . The extent of the segregation reaction and corresponding thermodynamic equilibrium will be addressed and discussed later. From Figure 2a, it can also be seen that segregation readily occurs even at room temperature despite the activation energy, calculated from the slope of the Arrhenius diagram, of  $32.0 \pm 3.8\text{ kJ mol}^{-1}$ . The obtained value is larger than that of  $\text{PEA Pb}(\text{Br}_{0.5}\text{I}_{0.5})_4$  ( $21.7\text{ kJ mol}^{-1}$ ),<sup>26</sup> which has shown negligible halide segregation under 1 sun.

In addition to temperature, excitation intensity has been shown to have an important effect on the photoinduced halide segregation processes. Threshold excitation intensity was introduced to explain the absence of segregation at low intensity (in a range from  $\sim 20$  to  $230\ \mu\text{W cm}^{-2}$ ).<sup>17,18</sup> On the other hand, it was reported that the segregated phases remixed at high intensity ( $0.75$  to  $200\text{ W cm}^{-2}$ ).<sup>39,40</sup> To elucidate the effect of excitation intensity on the photoinduced segregation processes in the  $\text{PPA}_2\text{Pb}(\text{Br}_{0.5}\text{I}_{0.5})_4$  films, we further investigated the segregation processes at moderate light intensities in between the low and high intensity extremes commonly investigated in the literature, i.e., with illumination intensities of  $9.5$  and  $12.0\text{ mW cm}^{-2}$ . From Figure 2b,c, we observe that the increase in intensity significantly affects the segregation

process at  $T = 25^\circ\text{C}$ , while the impact of intensity on the segregation occurring at  $T = 84^\circ\text{C}$  is insignificant.

The *in situ* absorption spectra, absorption difference spectra, and segregation traces recorded at different times during the segregation process of  $\text{PPA}_2\text{Pb}(\text{Br}_{0.5}\text{I}_{0.5})_4$  at  $T = 41, 56, 71,$  and  $84^\circ\text{C}$  under an illumination of  $9.5$  and  $12.0\text{ mW cm}^{-2}$  are shown in Figures S8 and S9, respectively. The obtained rate constants were presented in Figure 3a and Table S1. At low temperature, the increase of intensity significantly accelerates the segregation process. This is expected since the higher excitation power assists in overcoming the activation barrier.<sup>7</sup> However, with the increase in temperature, at  $T = 56$  and  $71^\circ\text{C}$ , the impact of increased intensity on the rate of segregation gradually diminishes. Finally, at  $T = 84^\circ\text{C}$ , photoinduced segregation processes under all three illuminating conditions almost have the same rate. Furthermore, it is important to notice that, under the illumination of  $6.5\text{ mW cm}^{-2}$ , the rate of reaction in the whole temperature range strongly depends on the temperature. However, for  $9.5$  and  $12.0\text{ mW cm}^{-2}$ , the segregation rates do not depend on temperature in the range from  $25$  to  $\sim 70^\circ\text{C}$ . In short, the kinetics of the segregation reactions under  $6.5\text{ mW cm}^{-2}$  is temperature-driven, while in the case of increased intensity, the kinetics of segregation is primarily determined by the intensity. Although the rate constant at  $12\text{ mW cm}^{-2}$  is comparable to that at  $84^\circ\text{C}$  and  $6.5\text{ mW cm}^{-2}$  ( $3.36 \times 10^{-3}\text{ s}^{-1}$ ), PHS is readily observed in the former, while it is absent in the later. This result clearly

differentiates kinetic and thermodynamic properties of PHS in our sample.

Figure 3b–d shows Arrhenius diagrams for the segregation reactions under  $6.5, 9.5,$  and  $12.0\text{ mW cm}^{-2}$ . We can observe that, at higher excitation ( $9.5$  and  $12\text{ mW cm}^{-2}$ ), the observed dependence can no longer be described with a single linear function. This indicates that additional mechanisms start to dominate the reaction, and consequently, we can distinguish two different regions at high temperature (temperature dominated region, TDR) and low temperature (light dominated region, LDR). The data in each region were fitted by a straight line, and for the TDR, one additional temperature data point was added. The activation energy for the segregation under  $6.5\text{ mW cm}^{-2}$  is  $32.0 \pm 3.8\text{ kJ mol}^{-1}$ . For

both 9.5 and 12 mW cm<sup>-2</sup>, activation energies in the TDR are of the same order of magnitude as at lower power (91 ± 29 and 42.1 ± 1.5 kJ mol<sup>-1</sup>, respectively), while in LDR, the activation energy is reduced by an order of magnitude; i.e., low values of 3.5 ± 0.8 and 3.6 ± 2.2 kJ mol<sup>-1</sup> are obtained. This suggests that the shift from the temperature-dependent regime to the intensity regime remarkably reduces the activation energy. In the intensity regime, an increase of the intensity mainly results in the increase of the reaction rate with only a slight change of activation energy.

Finally, we address the thermodynamic aspects of photo-induced segregation processes in the PPA<sub>2</sub>Pb(Br<sub>0.5</sub>I<sub>0.5</sub>)<sub>4</sub> films. If the photoinduced segregation process described by eq 1 is assumed to be reversible, the reaction will approach an equilibrium state at infinite time (Figure S10):

$$\frac{k}{2MFB + I} = \frac{k'}{K} \quad (3)$$

Therefore, the equilibrium constant ( $K_{\text{eq}}$ ) can be defined as

$$K_{\text{eq}} = \frac{[B] \times [I]}{[M]^2} = \frac{a_{\text{BaI}}}{a_{\text{m}}^2} \quad (4)$$

with the assumption that  $a_j = \gamma_j x_j$  with  $x_j$  being the molar fraction and  $\gamma_j = 1$ . In practice, we can define  $x/2 = x_{\text{B}} = x_{\text{I}}$  and  $x_{\text{M}} = 1 - x$  so that

$$K_{\text{eq}} = \frac{x^2}{4(1 - x)^2} \quad (5)$$

We assume that the molar fraction is proportional to the change in absorption, e.g.,  $x = \frac{\Delta \text{Abs}_m}{\text{Abs}_{0,m}}$ , where  $\text{Abs}_{0,m}$  and  $\Delta \text{Abs}_m$  are the initial absorbance of the mixed phase and the change in absorbance, respectively.  $\Delta \text{Abs}_m$  was obtained from the pre-exponential factor in the kinetic curve fitting while  $\text{Abs}_{0,m}$  was obtained from the peak area of the exciton peak in the mixed phase. The obtained  $K_{\text{eq}}$  values are presented in Figure 3e and Table S2. At  $T = 25$  °C, with the increase in intensity, the equilibrium is strongly shifted toward the mixed parent structure. However, with the further increase in temperature, at  $T = 56$  and  $71$  °C, the impact of the increased intensity on the equilibrium is gradually reduced. Finally, at  $T = 84$  °C, the equilibrium under all three illuminating conditions is almost the same. It is important to notice that, under the illumination of 6.5 mW cm<sup>-2</sup>, the equilibrium in the whole temperature range strongly depends on the temperature (as it is valid for the rate of segregation). With the increase in temperature, the equilibrium shifts toward the mixed phase. This is meaningful because the reaction entropy change, expected to be quite relevant in this process, will dominate at large  $T$  values. However, for 9.5 and 12.0 mW cm<sup>-2</sup>, the equilibrium is weakly temperature dependent in the range from 25 to 71 °C, similar to the observed two distinct regions in Arrhenius plots.

Additionally, we can consider enthalpy changes calculated from the Van't Hoff diagram for the segregation process at different intensities. A plot of  $\ln(K_{\text{eq}})$  vs  $1/T$  is shown in Figure 3f–h, and the linear curve is described by the Van't Hoff equation as follows

$$\ln(K_{\text{eq}}) = -\frac{\Delta H}{RT} + \frac{\Delta S}{R} \quad (6)$$

where  $\Delta H$  and  $\Delta S$  are the enthalpy change and the entropy change of PHS. Data at higher temperatures for 9.5 and 12 mW cm<sup>-2</sup> (TDR) have been fitted separately, as the reaction under these illumination intensities can no longer be described as a single linear function. The enthalpy change under 6.5 mW cm<sup>-2</sup> is  $-152 \pm 9$  kJ mol<sup>-1</sup>. The large negative value indicates that photoinduced segregation is a highly exothermic reaction, meaning that an increase in temperature shifts the equilibrium toward the mixed parent phase. For illumination intensities of 9.5 and 12 mW cm<sup>-2</sup> in the TDR, we observe enthalpy changes of  $-344 \pm 66$  and  $-197 \pm 87$  kJ mol<sup>-1</sup> in agreement with the behavior observed for lower illumination intensity. In the LDR, however, we observe a significant reduction of the enthalpy change to  $2 \pm 8$  and  $7 \pm 11$  kJ mol<sup>-1</sup>. The obtained uncertainties in this region are comparable to the uncertainty obtained for 6.5 mW/cm<sup>2</sup>, but due to the low values of  $\Delta H$  resulting from a weak dependence on temperature (dependence close to the horizontal line), the relative uncertainties of the parameters are large. A low enthalpy change suggests that the shift from the temperature-dependent regime to the intensity regime results in a significant decrease in the magnitude of heat release. In the intensity regime, the increase of the intensity results in a significant decrease of the equilibrium constant with only a slight change in the amount of released heat. To elucidate the effects of light intensity, the enthalpy change and entropy change with different intensities are plotted in Figure S11a. The intensity driven equilibrium shift can be described by the entropy change, which was obtained from the y-intercept of the Van't Hoff diagram. The reaction entropy changed from  $-478 \pm 28$  J K<sup>-1</sup> mol<sup>-1</sup> for 6.5 mW cm<sup>-2</sup> to  $-1020 \pm 190$  and  $-597 \pm 249$  J K<sup>-1</sup> mol<sup>-1</sup> for 9.5 and 12 mW cm<sup>-2</sup>, respectively, in the TDR. The negative value reveals that the entropy in the mixed phase is larger than that in the segregated phases. Also, the equilibrium is shifted to the mixed state because the increased intensity magnifies the amount of entropy loss. In the LDR, however, the reaction entropy reduced to  $5 \pm 25$  and  $-2 \pm 33$  J K<sup>-1</sup> mol<sup>-1</sup> for 9.5 and 12 mW cm<sup>-2</sup>, respectively. In this case as well, the

uncertainties are similar to that obtained for 6.5 mW/cm<sup>2</sup> (likely limited by experimental uncertainties of our setup), but the low value of  $\Delta S$  results in a large relative uncertainty. The significant changes in entropy loss and large uncertainties of the fitted parameters illustrate that with the increase of illumination power the process can no longer be well described by a simple Van't Hoff model; i.e.,  $\Delta H$  and  $\Delta S$  are temperature dependent in this range. This illustrates that with an increase of the illumination power additional mechanisms become significant.

In parallel to  $K_{\text{eq}}$ , we can extract the Gibbs free energy that directly expresses if the reaction is shifted toward the reactant or the product. A full heatmap diagram of this quantity is shown in Figure S11b. The calculated reaction Gibbs free energy shifts from negative to positive with an increased temperature at 6.5 mW cm<sup>-2</sup>. It coincides with the thermodynamic-based model where the halide mixing/demixing process is temperature dependent.<sup>18-20</sup> On the other hand, an increase in illumination power is found to increase the Gibbs free energy and thus favor the mixing process. This observation hints that there is a remixing behavior of MHPs at strong illumination conditions.<sup>39-41</sup> We speculate that the observed shifts in  $k$  and  $K_{\text{eq}}$  are caused by light induced surface deformation<sup>42</sup> such as redistribution of the strain gradient<sup>40</sup> or microstructure evolution.<sup>41</sup> The

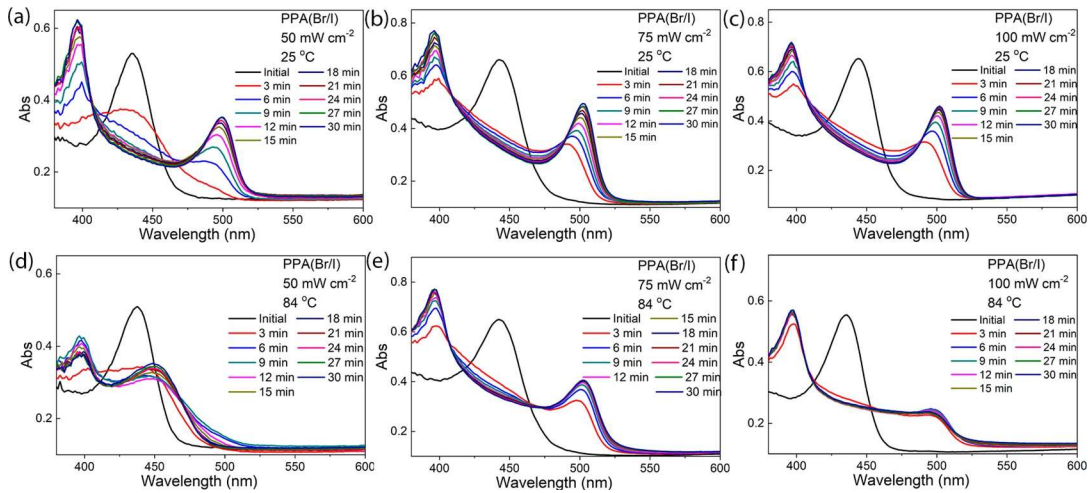


Figure 4. *In situ* absorption spectra of  $\text{PPA}_2\text{Pb}(\text{Br}_{0.5}\text{I}_{0.5})_4$  films at (a–c) 25 °C and (d–f) 84 °C for 30 min of illumination with white light intensities of (a, d)  $50 \text{ mW cm}^{-2}$  (b, e)  $75 \text{ mW/cm}^2$ , and (c, f)  $100 \text{ mW/cm}^2$ .

photothermal effect, which has been shown to remix segregated phases,<sup>41</sup> is excluded since the light intensity here is significantly lower than the reported power and the power-dependent effect fades at high temperature. However, it could play a role at higher illumination intensities, especially since the measured temperature increase of the sample using a thermocouple for the short duration of the experiment (30 min) may not necessarily reflect the localized heating of the perovskite layer due to low thermal conductivities of glass and MHPs.

The observed PHS process can be described by Gibbs free energy surface in Figure S11c. An equilibrium condition is established between the parent mixed phase and halide segregated phases. Under illumination, the populated photoexcited state features a free energy surface, which is favorable to the halide segregation. However, the shape of the ground free energy surface connecting the mixed and segregated phases ( $\Delta_r G^0$ ) depends on the temperature (Figure S11d). Entropy and enthalpy control the reaction equilibrium (and its behavior with temperature) while equilibration pathways take place regardless of illumination intensity. With increasing intensity, the PHS occurs faster because of the larger photoexcited population (effectively corresponding to a barrier reduction), but at the same time, the free energy difference is reduced, likely due to microstructure evolution, slightly affecting the properties of the reactant and product state. At a large intensity, the reaction is then shifted toward the mixed parent phase.

It should be noted that the observed trends (in terms of segregation and segregation suppression at a certain illumination intensity and/or temperature) are highly reproducible. However, the kinetics can vary from sample to sample, as illustrated in Figure S12. This is not surprising since the ion diffusion is dependent on native defects and grain boundaries, which are affected by the glovebox atmosphere at the time of synthesis, variations in manual application of antisolvent, etc. An important factor affecting the starting absorption spectrum and XRD pattern was found to be the use of different precursor combinations to obtain the films with the same final stoichiometry, as illustrated in Figure S13. It can be observed that there is a significant difference in the films prepared from  $2\text{PPABr}+\text{PbI}_2$  and  $2\text{PPAI}+\text{PbBr}_2$ , indicating that the precursors used affect the mixing in the final film with a shift possibly

occurring either due to internal strain or due to differences in mixing at nanoscale. Finally, it should be noted that at high illumination powers and/or temperatures the encapsulation of the samples plays an important role, since delamination can occur.<sup>43</sup> As shown in Figure S14, using a cover glass held together with clips (method previously reported<sup>18</sup>) results in an erroneous result of suppression of segregation (likely due to increased ion diffusion due to partial solvation due to moisture ingress), while segregation followed by remixing with a significant intensity drop is obtained with epoxy-only encapsulation, and finally, no remixing is observed when edges of the epoxy+cover glass encapsulated sample are additionally sealed by tape. At room temperature, epoxy+cover glass encapsulation is sufficient and reliable, but a simple cover glass held together with clips is not, as illustrated in Figure S15. This strongly indicates that the experimental investigations must be performed on properly encapsulated samples to ensure reproducibility.

Finally, while  $\text{PPA}_2\text{Pb}(\text{Br}_{0.5}\text{I}_{0.5})_4$  exhibits an interesting and unique dependence of PHS behavior at moderate light intensities, PHS under higher intensity (1 sun or  $100 \text{ mW/cm}^2$ ) is highly relevant for practical applications. Thus, we examined the behavior of  $\text{PPA}_2\text{Pb}(\text{Br}_{0.5}\text{I}_{0.5})_4$  under higher illumination power, as shown in Figure 4 as well as Figures S16–S18.

While photosegregation observed is strong at higher illumination intensities, different trends are observed for different illumination powers. At room temperature, the PHS is marked at 0.5 sun and even more at 0.75 and 1 sun. However, in all cases, illumination at 84 °C results in some suppression of the segregation. At 1 sun illumination, the segregation rate decreases with increasing temperature (Table S3), which is different from the observed temperature dependence at the low illumination intensity of  $6.5 \text{ mW/cm}^2$ . This led to a false estimation of activation energy with a negative value (Figure S19) and implies that the segregation consists of multistep processes under strong illumination. At the microscopic level, the increased light intensity will result in an increased photogenerated hole concentration with the hole trapping at the iodide sites potentially increasing lattice instability<sup>22</sup> and thus enhancing the segregation. For 0.5 sun illumination at 84 °C, we can observe some suppression of the segregation. We have already mentioned strain redistribution<sup>40</sup>

and microstructure evolution<sup>41</sup> as possible reasons for segregation suppression. Another possible connected phenomenon is the photostriction effect. It is known that MHPs exhibit a photostriction effect under illumination and the lattice compression saturates with increasing light intensity.<sup>44</sup> Since lattice compression increases the activation barrier for phase segregation,<sup>45</sup> this could contribute to the PHS suppression at light intensities with a further increase in the intensity and consequent increase in hole concentration, followed by increased hole trapping and polaron-related deformation, resulting in segregation dominance at high light intensity. The observed dependence of the PHS on temperature and light intensity indicates that additional mechanisms, different from the recognized processes (polaron-induced strain leading to the formation of I-rich domains, valence band edge variation, localization of holes at iodide sites, concentration gradients of halide species, defect involvement),<sup>32</sup> exist in these samples. These elements point to a different regime for the PHS compared to low illumination powers: as both internal and polaron-induced lattice strain can serve as driving forces for PHS,<sup>21</sup> we speculate that in some materials lattice compression can result in the suppression of PHS for certain light intensities. The coexistence of strain effects with other more general critical elements, such as hole and defects densities, may also play a role in approaching saturation regimes. Obtained results further suggest that the critical temperature for the photomiscibility gap (the temperature where segregation will stop) depends not only on the temperature but also on the interaction of material properties, the exposed environment, and the illumination condition.<sup>32</sup>

The observation of such an unusual dependence of PHS on light intensity and temperature in  $\text{PPA}_2\text{Pb}(\text{Br}_{0.5}\text{I}_{0.5})_4$  films highlights the need for comprehensive *in situ* characterizations, which will enable one to obtain information on structure/strain under illumination and at an elevated temperature, such as *in situ* XRD or Raman spectroscopy under white light illumination. At the same time, it is highly relevant to perform the measurements either for encapsulated samples or under an inert atmosphere since the presence of moisture and oxygen can not only cause degradation but also significantly alter the observed kinetics, likely due to higher ion mobility in the presence of moisture.

We studied the PHS process in the  $\text{PPA}_2\text{Pb}(\text{Br}_{0.5}\text{I}_{0.5})_4$  film with an *in situ* absorption measurement. The segregation process under Xe light was successfully captured without any interruption of remixing in the dark. Our observations indicate that the increase in temperature can result in the suppression of PHS despite the increase in the segregation rate with the increase in temperature. Also, we spotted the distinctive impacts of temperature and excitation intensity on PHS. At low intensity, the PHS process is primarily controlled by the temperature and the photoinduced segregation is hindered at high temperature because of its highly exothermic nature. An increase in the intensity to a moderate level ( $\sim 0.1$  sun) results in the emergence of dominance of other mechanisms, and consequently, more complex behavior is observed with two distinct regions distinguished in temperature dependence. Thus, under excitations of 9.5 and 12  $\text{mW}/\text{cm}^2$ , shifting of the equilibrium to the mixed state is observed. A further increase in intensity, however, results in segregation again becoming dominant at powers exceeding 0.5 sun, but at an illumination intensity of 1 sun, the segregation rate decreases with increasing temperature, which is different from the observed

behavior at a low illumination intensity of 6.5  $\text{mW}/\text{cm}^2$ . This complex dependence on the intensity and temperature highlights the need for the development of *in situ* characterization techniques as well as the necessity for further investigations utilizing different spacer cations to develop an improved understanding of PHS in layered halide perovskites.

## Supporting Information

Experimental details, absorption spectra of mixed halide perovskites with different spacer cations, absorption spectra and XRD patterns of  $\text{PPA}_2\text{PbBr}_4$ ,  $\text{PPA}_2\text{PbBr}_2\text{I}_2$ , and  $\text{PPA}_2\text{PbI}_4$ , spectrum of a Xe lamp and a comparison of an *in situ* absorption spectrum with that measured using an absorption spectrometer for  $\text{PPA}_2\text{PbBr}_2\text{I}_2$ , *in situ* absorption spectra and corresponding segregation traces for different powers and temperatures, enthalpy and entropy changes, Gibbs free energy reconstructed 2D heatmap and illustration of the behavior of the free energy reaction surface, effects of precursors used on film properties, effects of the encapsulation method on the photoinduced segregation behavior at 25 and 84 °C, and rate and equilibrium constants for different conditions (PDF)

- (1) Tao, S.; Schmidt, I.; Brocks, G.; Jiang, J.; Tranca, I.; Meerholz, K.; Olthof, S. Absolute energy level positions in tin- and lead-based halide perovskites. *Nat. Commun.* 2019, *10*, 2560.
- (2) Karlsson, M.; Yi, Z.; Reichert, S.; Luo, X.; Lin, W.; Zhang, Z.; Bao, C.; Zhang, R.; Bai, S.; Zheng, G.; Teng, P.; Duan, L.; Lu, Y.; Zheng, K.; Pullerits, T.; Deibel, C.; Xu, W.; Friend, R.; Gao, F. Mixed halide perovskites for spectrally stable and high-efficiency blue light-emitting diodes. *Nat. Commun.* 2021, *12*, 361.
- (3) Yuan, S.; Cui, L.-S.; Dai, L.; Liu, Y.; Liu, Q.-W.; Sun, Y.-Q.; Auras, F.; Anaya, M.; Zheng, X.; Ruggeri, E.; Yu, Y.-J.; Qu, Y.-K.; Abdi-Jalebi, M.; Bakr, O. M.; Wang, Z.-K.; Stranks, S. D.; Greenham, N. C.; Liao, L.-S.; Friend, R. H. Efficient and Spectrally Stable Blue Perovskite Light-Emitting Diodes Employing a Cationic  $\pi$ -Conjugated Polymer. *Adv. Mater.* 2021, *33* (11), 2103640.
- (4) Al-Ashouri, A.; Köhnen, E.; Li, B.; Magomedov, A.; Hempel, H.; Caprioglio, P.; Márquez José, A.; Morales Vilches Anna, B.; Kasparavicius, E.; Smith Joel, A.; Phung, N.; Menzel, D.; Grischek, M.; Kegelmann, L.; Skroblin, D.; Gollwitzer, C.; Malinauskas, T.; Jost, M.; Matic, G.; Rech, B.; Schlattmann, R.; Topic, M.; Korte, L.; Abate, A.; Stannowski, B.; Neher, D.; Stolterfoht, M.; Unold, T.; Getautis, V.; Albrecht, S. Monolithic perovskite/silicon tandem solar cell with > 29% efficiency by enhanced hole extraction. *Science* 2020, *370* (6522), 1300–1309.
- (5) Kamaraki, C.; Klug, M. T.; Green, T.; Perez, L. M.; Case, C. Perovskite/silicon tandem photovoltaics: Technological disruption without business disruption. *Appl. Phys. Lett.* 2021, *119* (7), 070501.
- (6) Wang, R.; Huang, T.; Xue, J.; Tong, J.; Zhu, K.; Yang, Y. Prospects for metal halide perovskite-based tandem solar cells. *Nat. Photonics* 2021, *15* (6), 411–425.
- (7) U.S. National Renewable Energy Laboratory *Best Research-Cell Efficiency Chart*; U.S. National Renewable Energy Laboratory, 2021.
- (8) Richter, A.; Hermle, M.; Glunz, S. W. Reassessment of the Limiting Efficiency for Crystalline Silicon Solar Cells. *IEEE J. Photovolt.* 2013, *3* (4), 1184–1191.
- (9) Hoke, E. T.; Slotcavage, D. J.; Dohner, E. R.; Bowering, A. R.; Karunadasa, H. I.; McGehee, M. D. Reversible photo-induced trap formation in mixed-halide hybrid perovskites for photovoltaics. *Chem. Sci.* 2015, *6* (1), 613–617.
- (10) Hu, L.; Guan, X.; Chen, W.; Yao, Y.; Wan, T.; Lin, C.-H.; Pham, N. D.; Yuan, L.; Geng, X.; Wang, F.; Huang, C.-Y.; Yuan, J.; Cheong, S.; Tilley, R. D.; Wen, X.; Chu, D.; Huang, S.; Wu, T. Linking Phase Segregation and Photovoltaic Performance of Mixed-Halide Perovskite Films through Grain Size Engineering. *ACS Energy Lett.* 2021, *6* (4), 1649–1658.
- (11) Yang, T. C.-J.; Fiala, P.; Jeangros, Q.; Ballif, C. High-Bandgap Perovskite Materials for Multijunction Solar Cells. *Joule* 2018, *2* (8), 1421–1436.
- (12) Yoon, S. J.; Kuno, M.; Kamat, P. V. Shift Happens. How Halide Ion Defects Influence Photoinduced Segregation in Mixed Halide Perovskites. *ACS Energy Lett.* 2017, *2* (7), 1507–1514.
- (13) Balakrishna, R. G.; Kobosko, S. M.; Kamat, P. V. Mixed Halide Perovskite Solar Cells. Consequence of Iodide Treatment on Phase Segregation Recovery. *ACS Energy Lett.* 2018, *3* (9), 2267–2272.
- (14) Brivio, F.; Caetano, C.; Walsh, A. Thermodynamic Origin of Photoinstability in the  $\text{CH}_3\text{NH}_3\text{Pb}(\text{I}_{1-x}\text{Br}_x)_3$  Hybrid Halide Perovskite Alloy. *J. Phys. Chem. Lett.* 2016, *7* (6), 1083–1087.
- (15) Bischak, C. G.; Hetherington, C. L.; Wu, H.; Aloni, S.; Ogletree, D. F.; Limmer, D. T.; Ginsberg, N. S. Origin of Reversible Photoinduced Phase Separation in Hybrid Perovskites. *Nano Lett.* 2017, *17* (2), 1028–1033.
- (16) Draguta, S.; Sharia, O.; Yoon, S. J.; Brennan, M. C.; Morozov, Y. V.; Manser, J. M.; Kamat, P. V.; Schneider, W. F.; Kuno, M. Rationalizing the light-induced phase separation of mixed halide organic-inorganic perovskites. *Nat. Commun.* 2017, *8*, 200.
- (17) Ruth, A.; Brennan, M. C.; Draguta, S.; Morozov, Y. V.; Zhukovskiy, M.; Janko, B.; Zapol, P.; Kuno, M. Vacancy-Mediated Anion Photo-segregation Kinetics in Mixed Halide Hybrid Perovskites: Coupled Kinetic Monte Carlo and Optical Measurements. *ACS Energy Lett.* 2018, *3* (10), 2321–2328.
- (18) Elmelund, T.; Seger, B.; Kuno, M.; Kamat, P. V. How Interplay between Photo and Thermal Activation Dictates Halide Ion Segregation in Mixed Halide Perovskites. *ACS Energy Lett.* 2020, *5* (1), 56–63.
- (19) Wang, X.; Ling, Y. C.; Lian, X. J.; Xin, Y.; Dhungana, K. B.; Perez-Orive, F.; Knox, J.; Chen, Z. Z.; Zhou, Y.; Beery, D.; Hanson, K.; Shi, J.; Lin, S. C.; Gao, H. W. Suppressed phase separation of mixed-halide perovskites confined in endotaxial matrices. *Nat. Commun.* 2019, *10*, 695.
- (20) Pavlovets, I. M.; Ruth, A.; Gushchina, I.; Ngo, L.; Zhang, S. B.; Zhang, Z. M.; Kuno, M. Distinguishing Models for Mixed Halide Lead Perovskite Photo-segregation via Terminal Halide Stoichiometry. *ACS Energy Lett.* 2021, *6* (6), 2064–2071.
- (21) Choe, H.; Jeon, D.; Lee, S. J.; Cho, J. Mixed or Segregated: Toward Efficient and Stable Mixed Halide Perovskite-Based Devices. *ACS Omega* 2021, *6*, 24304–24315.
- (22) DuBose, J. T.; Kamat, P. V. Hole Trapping in Halide Perovskites Induces Phase Segregation. *Acc. Mater. Res.* 2022, *3*, 761–771.
- (23) Xiao, Z.; Zhao, L.; Tran, N. L.; Lin, Y. L.; Silver, S. H.; Kerner, R. A.; Yao, N.; Kahn, A.; Scholes, G. D.; Rand, B. P. Mixed-Halide Perovskites with Stabilized Bandgaps. *Nano Lett.* 2017, *17* (11), 6863–6869.
- (24) Zhou, Y.; Wang, F.; Cao, Y.; Wang, J.-P.; Fang, H.-H.; Loi, M. A.; Zhao, N.; Wong, C.-P. Benzylamine-Treated Wide-Bandgap Perovskite with High Thermal-Photostability and Photovoltaic Performance. *Adv. Energy Mater.* 2017, *7* (22), 1701048.
- (25) Mathew, P. S.; DuBose, J. T.; Cho, J. S.; Kamat, P. V. Spacer Cations Dictate Photoinduced Phase Segregation in 2D Mixed Halide Perovskites. *ACS Energy Lett.* 2021, *6* (7), 2499–2501.
- (26) Cho, J.; Mathew, P. S.; DuBose, J. T.; Kamat, P. V. Photoinduced Halide Segregation in Ruddlesden-Popper 2D Mixed Halide Perovskite Films. *Adv. Mater.* 2021, *33* (48), 2105585.
- (27) Wang, Y.-R.; Senocrate, A.; Mladenovic, M.; Ducinskis, A.; Kim, G. Y.; Rothlisberger, U.; Milic, J. V.; Moia, D.; Grätzel, M.; Maier, J. Photo De-Mixing in Dion-Jacobson 2D Mixed Halide Perovskites. *Adv. Energy Mater.* 2022, *12*, 2200768.
- (28) Cho, J.; DuBose, J. T.; Le, A. N. T.; Kamat, P. V. Suppressed Halide Ion Migration in 2D Lead Halide Perovskites. *ACS Materials Lett.* 2020, *2*, 565–570.
- (29) Liu, Y.; Wang, M.; Ievlev, A. V.; Ahmadi, A.; Keum, J. K.; Ahmadi, M.; Hu, B.; Ovchinnikova, O. S. Photoinduced iodide repulsion and halides-demixing in layered perovskites. *Mater. Today Nano* 2022, *18*, 100197.
- (30) Shi, E.; Yuan, B.; Shiring, S. B.; Gao, Y.; Akriti; Guo, Y.; Su, C.; Lai, M.; Yang, P.; Kong, J.; Savoie, B. M.; Yu, Y.; Dou, L. Two-dimensional halide perovskite lateral epitaxial heterostructures. *Nature* 2020, *580*, 614–620.
- (31) Brennan, M. C.; Draguta, S.; Kamat, P. V.; Kuno, M. Light-Induced Anion Phase Segregation in Mixed Halide Perovskites. *ACS Energy Lett.* 2018, *3* (1), 204–213.
- (32) Wang, Y. R.; Kim, G. Y.; Kotomin, E.; Moia, D.; Maier, J. Photo de-mixing in mixed halide perovskites: the roles of ions and electrons. *J. Phys. Energy* 2022, *4*, 011001.
- (33) Polyzoidis, C.; Rogdakis, K.; Kymakis, E. Indoor Perovskite Photovoltaics for the Internet of Things—Challenges and Opportunities toward Market Uptake. *Adv. Energy Mater.* 2021, *11*, 2101854.

- (34) Muhammad, B. T.; Kar, S.; Stephen, M.; Leong, W. L. Halide perovskite-based indoor photovoltaics: recent development and challenges. *Materials Today Energy* 2022, 23, 100907.
- (35) Du, K.-Z.; Tu, Q.; Zhang, X.; Han, Q.; Liu, J.; Zauscher, S.; Mitzi, D. B. Two-Dimensional Lead(II) Halide-Based Hybrid Perovskites Templated by Acene Alkylamines: Crystal Structures, Optical Properties, and Piezoelectricity. *Inorg. Chem.* 2017, 56 (15), 9291–9302.
- (36) Gong, X.; Voznyy, O.; Jain, A.; Liu, W.; Sabatini, R.; Piontkowski, Z.; Walters, G.; Bappi, G.; Nokhrin, S.; Bushuyev, O.; Yuan, M.; Comin, R.; McCamant, D.; Kelley, S. O.; Sargent, E. H. Electron-phonon interaction in efficient perovskite blue emitters. *Nat. Mater.* 2018, 17, 550–556.
- (37) Knight, A. J.; Wright, A. D.; Patel, J. B.; McMeekin, D. P.; Snaith, H. J.; Johnston, M. B.; Herz, L. M. Electronic Traps and Phase Segregation in Lead Mixed-Halide Perovskite. *ACS Energy Lett.* 2019, 4 (1), 75–84.
- (38) Bischak, C. G.; Wong, A. B.; Lin, E.; Limmer, D. T.; Yang, P.; Ginsberg, N. S. Tunable Polaron Distortions Control the Extent of Halide Demixing in Lead Halide Perovskites. *J. Phys. Chem. Lett.* 2018, 9 (14), 3998–4005.
- (39) Guo, Y. X.; Yin, X. T.; Liu, D.; Liu, J.; Zhang, C.; Xie, H. X.; Yang, Y. W.; Que, W. X. Photoinduced Self-healing of Halide Segregation in Mixed-halide Perovskites. *ACS Energy Lett.* 2021, 6 (7), 2502–2511.
- (40) Mao, W. X.; Hall, C. R.; Bernardi, S.; Cheng, Y. B.; Widmer-Cooper, A.; Smith, T. A.; Bach, U. Light-induced reversal of ion segregation in mixed-halide perovskites. *Nat. Mater.* 2021, 20, 55–61.
- (41) Vicente, J. R.; Kordesch, M. E.; Chen, J. Stabilization of mixed-halide lead perovskites under light by photothermal effects. *J. Energy Chem.* 2021, 63, 8–11.
- (42) Leng, K.; Abdelwahab, I.; Verzhbitskiy, I.; Telychko, M.; Chu, L.; Fu, W.; Chi, X.; Guo, N.; Chen, Z.; Chen, Z.; Zhang, C.; Xu, Q.-H.; Lu, J.; Chhowalla, M.; Eda, G.; Loh, K. P. Molecularly thin two-dimensional hybrid perovskites with tunable optoelectronic properties due to reversible surface relaxation. *Nat. Mater.* 2018, 17, 908–914.
- (43) Wang, Y.; Ahmad, I.; Leung, T.; Lin, J.; Chen, W.; Liu, F.; Ng, A. M. C.; Zhang, Y.; Djurišić, A. B. Encapsulation and Stability Testing of Perovskite Solar Cells for Real Life Applications. *ACS Mater. Au* 2022, 2 (3), 215–236.
- (44) Wei, T. C.; Wang, H. P.; Li, T. Y.; Lin, C. H.; Hsieh, Y. H.; Chu, Y. H.; He, J. H. Photostriction of  $\text{CH}_3\text{NH}_3\text{PbBr}_3$  Perovskite Crystals. *Adv. Mater.* 2017, 29, 1701789.
- (45) Muscarella, L. A.; Hutter, E. M.; Wittmann, F.; Woo, Y. W.; Jung, Y. K.; McGovern, L.; Versluis, J.; Walsh, A.; Bakker, H. J.; Ehrler, B. Lattice Compression Increases the Activation Barrier for Phase Segregation in Mixed-Halide Perovskites. *ACS Energy Lett.* 2020, 5, 3152–3158.

